

Article

Recycled Polypropylene/Strontium Ferrite Polymer Composite Materials with Electromagnetic Shielding Properties

Alina Ruxandra Caramitu ¹, Magdalena Valentina Lungu ¹, Romeo Cristian Ciobanu ^{2,*}, Ioana Ion ¹, Mihai Marin ¹, Virgil Marinescu ¹, Jana Pintea ¹, Sebastian Aradoaei ² and Oliver Daniel Schreiner ²

¹ National Institute for Research and Development in Electrical Engineering ICPE—CA Bucharest, 030138 Bucharest, Romania; alina.caramitu@icpe-ca.ro (A.R.C.); magdalena.lungu@icpe-ca.ro (M.V.L.); ioana.ion@icpe-ca.ro (I.I.); mihai.marin@icpe-ca.ro (M.M.); virgil.marinescu@icpe-ca.ro (V.M.); j_pintea@yahoo.com (J.P.)

² Department of Electrical Measurements and Materials, Gheorghe Asachi Technical University, 700050 Iasi, Romania; sebastian-teodor.aradoaei@academic.tuiasi.ro (S.A.); oliver-daniel.schreiner@academic.tuiasi.ro (O.D.S.)

* Correspondence: r.c.ciobanu@tuiasi.ro; Tel.: +40-751-164-501

Abstract: This paper presents the obtaining and characterization of recycled polypropylene/strontium ferrite (PP/SrFe₁₂O₁₉) polymer composite materials with applications in the electromagnetic shielding of vehicle interiors (mainly automotive electronics—carcasses) from the electromagnetic radiation emitted mainly by exterior sources—electrical lines and supply sources—in terms of the development of the new electrical vehicles. With this aim, suitable polymer composite materials were developed using SrFe₁₂O₁₉ filler in two forms (powder and concentrate). The recycled PP polymer and composite materials with a PP/SrFe₁₂O₁₉ weight ratio of 75/25 and 70/30 were obtained in two stages, i.e., pellets by extrusion and samples for testing through a melt injection process. The characterization of the obtained materials took into account the requirements imposed by the desired applications. It consisted of determining the mechanical and dielectric properties, and microstructure analyses, along with the determination of the resistance to the action of a temperature of 70 °C, which is higher than the temperatures created during the summer inside vehicles. The performance of these materials as electromagnetic shields was assessed through functional tests consisting of the determination of magnetic permeability and the estimation of the electromagnetic shielding efficiency (SE). The obtained results confirmed the improvement of the mechanical, dielectric, and magnetic properties of the PP/SrFe₁₂O₁₉ composites compared to the selected PP polymers. It is also found that all the composite materials exhibited reflective shielding properties (SE_R from −71.5 dB to −56.7 dB), with very little absorption shielding. The most performant material was the composite made of PP/SrFe₁₂O₁₉ powder with a weight ratio of 70/30. The promising results recommend this composite material for potential use in automotive shielding applications against electromagnetic pollution.

Keywords: polypropylene/strontium ferrite; PP/SrFe₁₂O₁₉; polymer composite; electromagnetic radiation; magnetic permeability; reflection shielding



Citation: Caramitu, A.R.; Lungu, M.V.; Ciobanu, R.C.; Ion, I.; Marin, M.; Marinescu, V.; Pintea, J.; Aradoaei, S.; Schreiner, O.D. Recycled Polypropylene/Strontium Ferrite Polymer Composite Materials with Electromagnetic Shielding Properties. *Polymers* **2024**, *16*, 1129. <https://doi.org/10.3390/polym16081129>

Academic Editors: Alexander Böker and Frank Wiesbrock

Received: 15 November 2023

Revised: 21 February 2024

Accepted: 15 April 2024

Published: 17 April 2024



Copyright: © 2024 by the authors. Licensee MDPI, Basel, Switzerland. This article is an open access article distributed under the terms and conditions of the Creative Commons Attribution (CC BY) license (<https://creativecommons.org/licenses/by/4.0/>).

1. Introduction

With recent advances in electromagnetic interference (EMI) shielding technologies and the rapid expansion of various electronic applications in the automotive industry, electromagnetic pollution has been steadily increasing. Electromagnetic waves can penetrate nearby electronic devices and adversely affect them or cause them to malfunction. With the increase in the number of electronically controlled automobile parts, accidents such as the malfunctioning and/or sudden acceleration of vehicles due to electromagnetic waves have become a major problem. Since electromagnetic waves can also harm people, the most effective EMI shielding technologies have demanded increased attention [1,2]. Electromagnetic radiation pollution can lead to damage to human health [2–11] and living matter [12–16],

so it is urgently necessary to reduce it by researching and designing different new materials effective for this purpose. These materials must synergistically ensure a good attenuation of electromagnetic waves [17,18] and high resistance to the action of fungi [12–16,19,20], environmental conditions [21–26], mechanical stresses [27,28], excellent dielectric, magnetic and electromagnetic characteristics [29–32], and high resistance to the action of microwaves and UV radiation [33]. These conditions can be ensured through polymer-based composite materials, which have excellent mechanical properties and thermal stability, as well as high resistance to environmental conditions. The most used fillers for the realization of composite materials applied as protective shields for electromagnetic waves are metal powders (e.g., Cu, Ni, Ag, Al, Au, among others) [34], or ferrite powders such as (Zn, Fe, Ni, Mg, Cd)Fe₂O₄ with crystallite sizes below 30 nm, which present exceptional shielding properties [34–36]. For instance, the ferrite/polymer composite material developed by Radoń et al. [30] exhibited in the frequency range of 1.9–2.1 GHz a reflection shielding efficiency (RL) lower than –25 dB and a shielding effectiveness (SE) lower than –50 dB for a 0.8–1 cm thick layer.

Compared to spinel ferrites, hexagonal ferrites are also of significant interest as high-frequency microwave-absorbing materials due to their in-plane magnetic anisotropy and natural resonance in the GHz range. M-type strontium ferrites (SrFe₁₂O₁₉) and barium ferrites (Fe₁₂BaO₁₉) are typical examples of the hexagonal group that exhibit significant uniaxial anisotropy and strong saturation magnetization [37,38].

Some researchers [36] incorporated Mn- and Ti-doped strontium hexaferrite (SrFe₉Mn_{1.5}Ti_{1.5}O₁₉) powders with a magnetoplumbite structure into a polyvinylchloride (PVC) matrix in mass concentrations of 50%, 60%, 70%, and 80%. The PVC/ferrite polymer composites were obtained via hot pressing at 220 °C and 5.5 MPa in the form of discs with a diameter of 40 mm and a thickness of 1.8 mm. The composite filled with 70 wt.% ferrite showed a reflection loss below –15 dB in the frequency range of 16.4–19.4 GHz, and a good microwave absorption performance in the frequency range of 8–18 GHz.

Over the years, there has been research achieved to obtain composite materials using rubber as a polymer matrix and a compound ferrite of Cr and Mn as a filler material [31,39,40]. These polymer composite materials find their usefulness in the absorption of microwaves in the frequency range of 3–12 GHz. On the other hand, rubber magnetic composites containing Sr ferrite and Ba ferrite were obtained for use in manufacturing permanent magnets [39,41,42]. In another study [38], polymer composites made of 55 vol.% Sr-ferrite powder, 30 vol.% polypropylene (PP), and a certain polyethylene glycol (PEG) binder system were processed by the powder injection molding (PIM), then the binders were removed via extraction and thermal debinding, and the obtained samples were further sintered to prepare Sr-ferrite-based permanent magnets. Most of the research carried out so far on these composite materials has been focused on improving the performance of permanent magnets. On the other hand, ferrite polymer nanocomposites (NCPs) are of great interest as EMI shielding materials over a wide range of frequencies due to their good dielectric and mechanical properties, lightweight, and reduced cost [43].

This paper presents the obtaining and characterization of PP/SrFe₁₂O₁₉ polymer composite materials with applications in the electromagnetic shielding of vehicle interiors (mainly automotive electronics—carcasses) from the electromagnetic radiation emitted mainly by exterior sources—electrical lines and supply sources—in terms of the development of the new electrical vehicles. The PP polymer and composite materials with a PP/SrFe₁₂O₁₉ weight ratio of 75/25 and 70/30 were obtained in two stages, i.e., pellets via extrusion and samples for testing through a melt injection process. The characterization of the obtained materials consisted of carrying out specific tests to determine the physical, mechanical, dielectric, magnetic, and electromagnetic properties, as well as the resistance to the effect of temperature, and microstructure analysis, to select the most performant materials for the use as electromagnetic shields. The originality of our work consists of the selection of the polymer matrix and the filler, as well as the concentrations chosen to obtain the proposed composite materials. The purpose of this work was to obtain a lightweight

polymer composite material with a reflection shielding efficiency (SE_R) lower than -30 dB with applications against electromagnetic pollution.

2. Materials and Methods

2.1. Materials

The raw materials used to obtain the polymer composite materials are as follows:

- Polypropylene obtained from recycling from electronic waste [44] with the properties shown in Table 1. The use of recycled polypropylene is in line with the Directive 2000/53/EU on end-of-life vehicles.
- $SrFe_{12}O_{19}$ powder acquired from TODA Ferrite (Korea) with the properties shown in Table 2. One important reason for choosing strontium ferrites is that they are low-cost, widely used for ferrite permanent magnets, and may also become an important source of recycled matter in the near future.
- $SrFe_{12}O_{19}$ concentrate of F1 type acquired from Mate Co., Ltd. (Wake, Japan) with the trade name HM 1213-PA12 + 85% $SrFe_{12}O_{19}$ and the properties shown in Table 3.

Table 1. Properties of polypropylene obtained from recycling from electronic waste.

Property Name	Standard	Property Value
Melt flow index (230 °C/2.16 kg)	ISO 1133 [45]	25 g/10 min
Density	ISO 1183 [46]	0.9 g/cm ³
Vicat softening temperature (condition A120)	ISO 306 [47]	150 °C
Tensile stress at yield	ASTM D638 [48]	33 MPa
Charpy impact strength (23 °C/notched)	ISO 179 [49]	2.5 kJ/m ²
Flexural modulus	ISO 178 [50]	1400 MPa

Table 2. Properties of $SrFe_{12}O_{19}$ powder.

Property Name	Property Value
Particle diameter	<1.05 μ m
Molecular weight	1061.7 g/mol
Melting point	>450 °C (mL)
Density	5.18 g/mL at 25 °C (mL)
Solubility	Soluble in organic solvents

Table 3. Properties of F1-type $SrFe_{12}O_{19}$ concentrate.

Property Name	Property Value
Specific gravity	3.2 g/cm ³
Melting point	190 °C
Residual magnetic field strength	235 mT
Coercive force	177 kA/m
Intrinsic coercive force	251 kA/m
Maximum stored energy	10.9 kJ/m ³
Density after ripening	3.21 g/cm ³
Melt flow index (270 °C/10 kg)	130 g/10 min
Bending strength	125 MPa
Impact strength	28 kJ/m ²

2.2. Equipment and Methods

2.2.1. Obtaining Polymer Composite Materials

Firstly, the component materials were homogenized through the mechanical mixing of the desired weight content of PP powder with $SrFe_{12}O_{19}$ powder/concentrate. The polymer composite materials were obtained in two stages, the first being composite pellets through extrusion, with the use of a laboratory twin screw extruder with PLC control type, Dongguan Baopin Precision Instruments Co., Ltd., Dongguan City, Guangdong Province

(China), a length/diameter (L/D) ratio of 1:40, a screw rotation speed up to 120 rpm, frequency control, 5 heating zones, soft water circulating cooling, vibration feeding method, vacuum pump, etc. Finally, the second stage includes samples for testing, via a melt injection process with a Dr. Boy 35A injection molding machine, Dr. Boy GmbH & Co. KG Neustadt-Fernthal, (Germany) with a screw diameter of 28 mm, a screw length/diameter (L/D) ratio of 18.6, a maximum clamping force of 350 kN, and a maximum working temperature of 300 °C. The concentrations of the obtained materials and their coding are presented in Table 4. Regarding the injection process, the working temperatures of 180–250 °C and clamping forces of 138–155 kN were used to achieve disc-shaped materials with a diameter of 30 ± 0.1 mm and a thickness of 2 ± 0.1 mm.

Table 4. Material compositions and coding.

Material Code	Composition (wt.%) of PP/SrFe ₁₂ O ₁₉ Powder	Composition (wt.%) of PP/SrFe ₁₂ O ₁₉ Concentrate
M0	100/0	-
M1	75/25	-
M2	70/30	-
M3	-	75/25
M4	-	70/30

2.2.2. Material Characterization

Density Determination

The density of the M0-M4 materials was determined with Archimedes' method in ethanol at 23 °C using an XS204 Mettler Toledo (Greifensee, Switzerland) hydrostatic balance equipped with a specific kit for solid materials, according to ASTM D792 standard [51]. Five specimens per material were measured and mean \pm standard deviation (SD) values of the hydrostatic density were reported together with the calculated relative density and porosity values. The theoretical density of the composite materials was calculated with the rule of mixture.

Mechanical Characterization

The mechanical properties of the M0-M4 materials were investigated using a Micro-Combi Tester (MCT²) equipped with a diamond Berkovich indenter (CSM Instruments, Peseux, Switzerland) and load-controlled instrumented indentation testing (IIT), according to ISO 14577-1 standard [52]. The IIT measurements were performed with a maximum load (F_{\max}) of 400 mN in a quadratic loading, a time to loading/unloading F_{\max} of 30 s, a hold time at F_{\max} of 10 s, an approach speed of the indenter of 2000 nm/min, and an acquisition rate of 10 Hz. The indentation hardness (H_{IT}), indentation elastic modulus (E_{IT}), contact stiffness (S), indentation creep (C_{IT}), elastic reverse and plastic deformation work of indentation (W_{elast} and W_{plast}), and elastic part of indentation work (η_{IT}) were determined via the Oliver and Pharr calculation method [53] as we detailed elsewhere [54] using a geometric factor (β) of 1.034 for the diamond Berkovich indenter with a Poisson's ratio (ν_i) of 0.07 and Young's modulus (E_i) of 1141 GPa, a Poisson's ratio of 0.42 for the PP material (M0), and 0.37 for the polymer composite materials (M1-M4). Five measurements were realized per sample and mean \pm standard deviation (SD) values were reported.

SEM Analyses

The microscopic structure and morphology investigation of the M0-M4 materials and filler materials (SrFe₁₂O₁₉ powder/concentrate) was performed with a field emission scanning electron microscope (FESEM), model Auriga (Carl Zeiss, Oberkochen, Germany), and a focused ion beam (FIB) column, model Canion (Orsay Physics, Fuveau, France). The SEM images were recorded on a cross-section of the solid samples and a charge compensation (CC) system, at an acceleration voltage of 5 kV with a secondary electron (SE) detector of Everhart Thornley type with a Faraday cup.

Thermal Analysis

The thermal analysis of the M0-M4 materials was conducted on an STA 449 F3 Jupiter thermal analyzer (Netzsch, Selb, Germany). The thermogravimetric (TG) and derivative thermogravimetric (DTG) curves of small amounts of material (10–15 mg) taken from each injection molded material and placed in 85 μL alumina (Al_2O_3) crucibles without lids were recorded in static air in the temperature range of 20–700 $^\circ\text{C}$ with a heating rate of 10 K/min.

Dielectric Characterization

The dielectric properties such as the real (ϵ') and imaginary parts (ϵ'') of relative permittivity, along with the tangent of the dielectric loss angle ($\text{tg } \delta = \epsilon'' / \epsilon'$) of the M0-M4 samples were determined via dielectric spectroscopy using a Solartron 1260A dielectric spectrometer (Solartron Analytical, Farnborough, UK). The measurements were recorded using an electric field of an AC voltage amplitude of 3 V over a frequency range of 8–30 MHz and a measuring electrode with a diameter of 30 mm, according to the equations presented, e.g., in [55].

Temperature Resistance Testing

The resistance to the effect of temperature on the M0-M4 samples was carried out by analyzing the variation of $\text{tg } \delta$ and electrical resistivity for the estimation of the critical resistivity and time. The critical value of the electrical resistivity at which the material is considered degraded was chosen at the moment when the electrical resistivity decreased to 30% of the initial value. All samples were heated in a Memmert oven model UF 55, Memmert GmbH + Co. KG., Schwabach (Germany) at 70 $^\circ\text{C}$ for 72 h then cooled in air at room temperature to measure $\text{tg } \delta$. This heating/cooling cycle was repeated 8 times. The selected temperature of 70 $^\circ\text{C}$ used in accelerated aging is higher than the temperature used inside vehicles.

Magnetic Characterization

The magnetic permeability of the M0-M4 samples was determined using a 4294A precision impedance analyzer (Agilent Technology Japan, Ltd., Tokyo, Japan) equipped with a 16454A Magnetic Material Test Fixture kit. Each sample was prepared as a hollow cylinder having an external diameter of 20 ± 0.1 mm, an internal diameter of 8 ± 0.1 mm, and a thickness of 2 ± 0.1 mm to measure the inductance at the ends of the wire. When the cylindrical sample is inserted into the Test Fixture kit, an ideal, single-turn inductor, with no flux leakage, is formed. Permeability is derived from the inductance of the core with the fixture. The real (μ') and imaginary parts (μ'') of magnetic permeability were determined from the inductance measurements over the frequency range of 8–30 MHz, according to the following equations [56,57]:

$$\mu' = \frac{lL_{eff}}{\mu_0 N^2 A} \quad (1)$$

$$\mu'' = \frac{l(R_{eff} - R_w)}{\mu_0 N^2 \omega A} \quad (2)$$

where l is the average length of the magnetic core, L_{eff} is the coil inductance, R_{eff} is the equivalent resistance of the magnetic core losses including the wire resistance, N is the number of windings, R_w is the wire resistance, A is the cross-sectional area of the magnetic core, ω is the angular frequency ($\omega = 2\pi f$), f is the linear frequency (Hz), and μ_0 is the permeability of vacuum ($\mu_0 = 4\pi \times 10^{-7}$ H/m).

3. Results and Discussion

3.1. Macrographic Aspect, Density, and Porosity

The macrographic aspect, along with the density and porosity of the M0-M4 materials obtained by injection molding is presented in Figure 1 and Table 5, respectively.

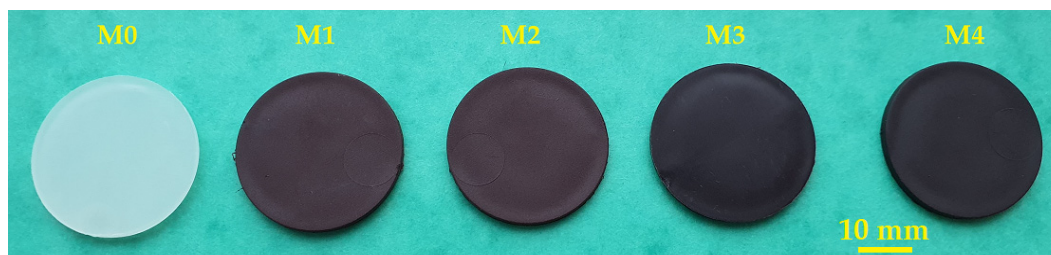


Figure 1. Macrographic aspect of the M0-M4 materials obtained through injection molding.

Table 5. Density and porosity of the M0-M4 materials obtained through injection molding.

Material Code	Theoretical Density (g/cm ³)	Mean Density \pm SD (g/cm ³)	Relative Density (%)	Porosity (%)
M0	0.900	0.894 \pm 0.002	99.33	0.67
M1	1.134	1.077 \pm 0.002	94.95	5.05
M2	1.197	1.157 \pm 0.002	96.69	3.31
M3	1.097	1.068 \pm 0.002	97.32	2.68
M4	1.148	1.138 \pm 0.019	99.15	0.85

The results regarding the aspect (Figure 1) and density (Table 5) show the obtaining of uniform and homogeneous polymer composite materials (M1-M4) through the mechanical mixing of the desired weight content of PP powder with SrFe₁₂O₁₉ powder/concentrate, and injection molding. The used preparation methods are in line with other literature reports [43,58,59]. Additionally, Weidenfeller et al. [58] disclosed that the addition of 30 vol.% SrFe₁₂O₁₉ powders to a PP matrix had a benefic effect on reducing the cooling time during the injection-molding process of the ferrite polymer composite.

In our study, the obtained density of the polymer composite materials ranges between 1.068 \pm 0.002 g/cm³ and 1.157 \pm 0.002 g/cm³ and increased in the series: M3, M1, M4, and M2. The materials with SrFe₁₂O₁₉ powder filler exhibited higher density than the materials with SrFe₁₂O₁₉ filler concentrate at the same content of filler. It is also noticed that the addition of SrFe₁₂O₁₉ powder/concentrate filler increased by about 20–29% the density of the PP/SrFe₁₂O₁₉ polymer composites (M1-M4) compared to the density of the PP polymeric material (M0). However, all the developed composite materials (M1-M4) meet the lightweight requirement for use as EMI shielding materials.

3.2. Mechanical Properties

In contrast to conventional polymeric materials, the mechanical properties of polymer composite materials can be mostly controlled by the choice of components, the percentage and type of addition in the matrix (binder), the geometry and orientation of the fillers, and the preparation methods of mixtures and their processing techniques and conditions. The mechanical characteristics of polymer composite materials are strongly dependent on the mechanical strength, hardness, and stiffness of the fillers, as they are higher than those of the polymeric materials used as a matrix [60].

An instrumented indentation technique (IIT) such as nanoindentation with a Berkovich diamond indenter has been utilized over the last twenty years for assessing the mechanical properties of polymer composite materials [61–63]. Furthermore, the calculation method employed in the IIT was introduced by Oliver and Pharr in 1992 [53]. It is widely used in data analysis for studying the mechanical behavior of solid surfaces, thin films, and coatings made of different materials [64].

Table 6 and Figure 2 present the experimental data obtained by nanoindentation and the Oliver and Pharr method for the studied composite materials.

Table 6. Mean \pm SD values of the mechanical properties (indentation hardness (H_{IT}), indentation elastic modulus (E_{IT}), contact stiffness (S), indentation creep (C_{IT}), elastic reverse deformation work of indentation (W_{elast}), plastic deformation work of indentation (W_{plast}), and elastic part of indentation work (η_{IT})) of the materials determined through nanoindentation and the Oliver and Pharr method.

Material Code	H_{IT} (GPa)	Vickers Hardness HV	E_{IT} (GPa)	S (mN/ μ m)	C_{IT} (%)	W_{elast} (μ J)	W_{plast} (μ J)	η_{IT} (%)
M0	0.081 ± 0.005	7.53 ± 0.44	1.03 ± 0.06	101.59 ± 3.80	8.04 ± 0.15	0.99 ± 0.02	1.65 ± 0.07	37.07 ± 0.57
M1	0.084 ± 0.005	7.74 ± 0.50	1.21 ± 0.05	112.51 ± 1.92	7.91 ± 0.37	0.91 ± 0.02	1.66 ± 0.05	35.25 ± 0.55
M2	0.094 ± 0.003	8.67 ± 0.32	1.34 ± 0.03	118.38 ± 1.83	9.04 ± 0.34	0.85 ± 0.01	1.73 ± 0.04	32.89 ± 0.59
M3	0.083 ± 0.003	7.69 ± 0.24	1.12 ± 0.03	104.71 ± 5.27	8.05 ± 0.28	0.98 ± 0.01	1.70 ± 0.06	36.52 ± 0.71
M4	0.089 ± 0.008	8.23 ± 0.75	1.17 ± 0.05	105.43 ± 2.88	8.07 ± 0.44	0.97 ± 0.02	1.66 ± 0.07	36.75 ± 1.02

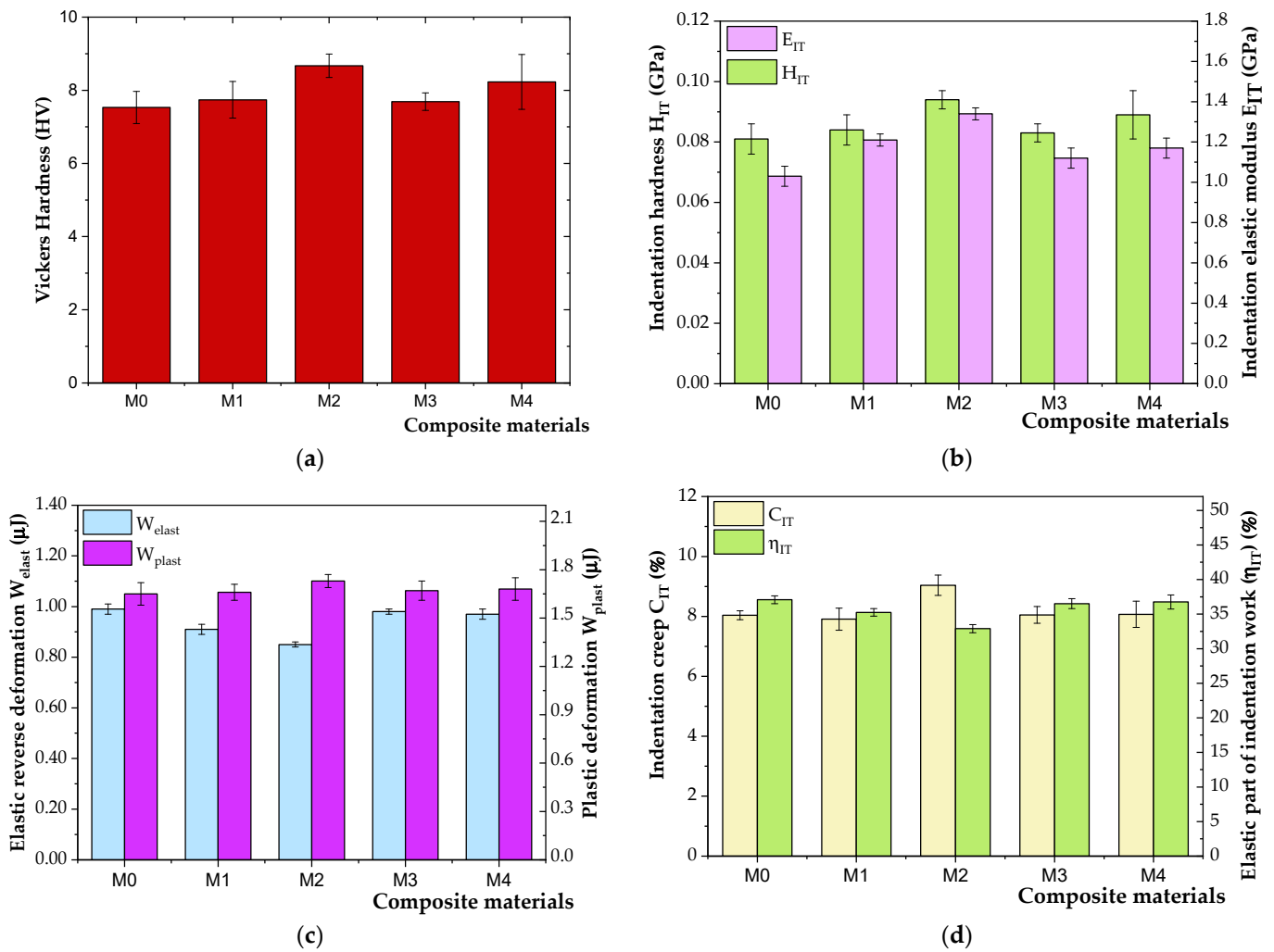


Figure 2. (a) Vickers hardness (HV); (b) indentation elastic modulus (E_{IT}) and indentation hardness (H_{IT}); (c) elastic reverse and plastic deformation (W_{elast} , and W_{plast}); and (d) indentation creep (C_{IT}) and elastic part of indentation (η_{IT}) of the studied materials.

In Table 6 and Figure 2, it is noticed that all the M1-M4 materials exhibited higher Vickers hardness HV ranging from 7.69 ± 0.24 to 8.67 ± 0.32 , and better resistance to permanent (plastic) deformation or damage (H_{IT} between 0.083 ± 0.003 GPa and 0.094 ± 0.003 GPa) compared to the PP polymer (M0) (HV of 7.53 ± 0.44 and H_{IT} values of 0.081 ± 0.005 GPa). Moreover, the composite materials with the highest percentage in $SrFe_{12}O_{19}$ filler of 30 wt.% (M2 and M4) have the highest H_{IT} and HV hardness, while the lowest hardness is presented by the PP polymer without filler (M0). Therefore, it can be concluded that both H_{IT} and

HV values increased for the M2 material by about 16% and 15%, respectively, by adding 30 wt.% SrFe₁₂O₁₉ powder filler in the PP matrix. The increase in the H_{IT} and HV values of the M4 material was about 11% and 9%, respectively, which is lower than for the M2 material due to the polyamide (PA) existent in the ferrite concentrate.

Regarding the indentation elastic modulus (E_{IT}), which is similar to Young's modulus, being determined from the slope of the unloading curve [65], it is found that the composite materials show higher E_{IT} (1.12 ± 0.03 GPa to 1.34 ± 0.03 GPa) than that of the PP polymer (1.03 ± 0.06 GPa). Additionally, the E_{IT} varies similarly to the trend of H_{IT} and HV. The E_{IT} results are in agreement with the results shown in the literature reports [66]. Polymers and polymer composites are generally found to have low E_{IT}, indicating high polymer crystallinity. The more crystalline a polymer is (the content of crystalline areas is higher), the physical–mechanical properties improve but the fragility increases [57]. The increase in the elastic modulus of the polymer composites due to the filler addition can result from a good adhesion of the filler with the polymer matrix without the formation of large agglomerates, or from the filler interference on the polymer crystallization [60].

The IIT results show that the highest values of contact stiffness (S) were measured on the M2 material with the highest filler content (118.38 ± 1.83 mN/μm), followed by the M1 material (112.51 ± 1.92 mN/μm), these materials being obtained with 30 wt.% or 25 wt.% SrFe₁₂O₁₉ powder filler. The addition of 25–30 wt.% SrFe₁₂O₁₉ concentrate to the PP matrix also improved the contact stiffness at about 105 ± 5 mN/μm, while the lowest S values of 101.59 ± 3.80 mN/μm were reached in the PP polymer (M0). The creep behavior of the M0, M3, and M4 materials with PP and 25–30 wt.% PP/SrFe₁₂O₁₉ concentrate is similar. In contrast, the M1 material with 25 wt.% SrFe₁₂O₁₉ powder yielded the best creep resistance, while the increase in the SrFe₁₂O₁₉ powder content from 25 wt.% to 30 wt.% led to an increase in the C_{IT} values by about 14%, indicating a larger creep deformation [66]. Moreover, the M2 material exhibited higher plastic behavior (W_{plast} of 1.73 ± 0.04 μJ, and the plastic part of the indentation work of 67.11 ± 0.59%) than the other materials. All the M0–M1 materials exhibited a similar viscoelastic behavior showing higher W_{plast} values than the W_{elast} ones, but these values varied in a narrow range. The PP polymer (M0) exhibited the highest W_{elast} and η_{IT} values indicating higher elastic deformation ability due to preserving the polymer chains structure in case no filler is added to the polymer matrix.

3.3. SEM Analysis

SEM analysis was carried out for all the materials obtained through injection molding, as well as for the filler raw materials used to obtain them. All the SEM images were recorded on the cross-section of the solid samples and the charge compensation (CC) system. The employed CC system uses an injection of nitrogen gas on a locally analyzed surface, which allows for the obtaining of images without metal deposition on the surfaces of analyzed samples. Hence, the true state of the morphology of the surfaces of samples is highlighted without inducing the formation of any artifacts to the analyzed areas but decreases the quality of images (low smoothing of surfaces due to charge effect which is still present). It also can decrease the contrast of the obtained images.

The micrographs of the SrFe₁₂O₁₉ powder and F1 concentrate are presented in Figure 3, and the micrographs of the M0–M4 materials are presented in Figure 4 and Figure 5, respectively.

In the microscopic images of the ferrite fillers (Figure 3), a large grain size distribution of the SrFe₁₂O₁₉ particles in the micrometer range (<1 μm) can be seen for the ferrite powder. On the other hand, the grain size distribution of the SrFe₁₂O₁₉ particles incorporated in the F1-type ferrite concentrate cannot be differentiated in the polyamide (PA) matrix.

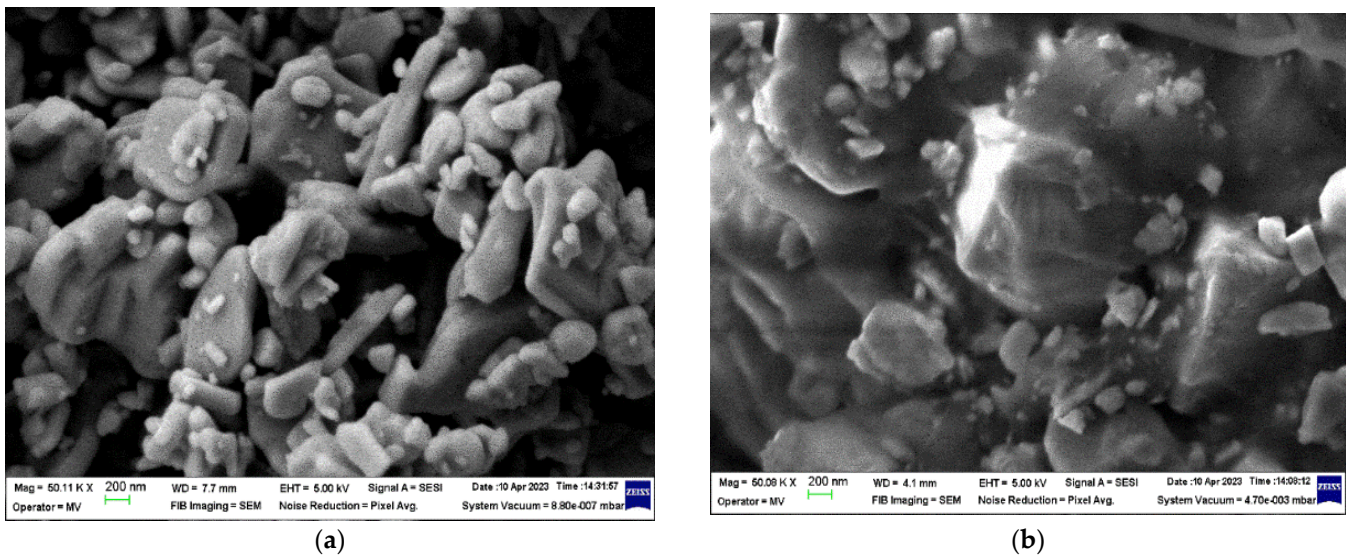


Figure 3. Microscopic images (50,000 \times) for (a) SrFe₁₂O₁₉ powder and (b) F1 concentrate.

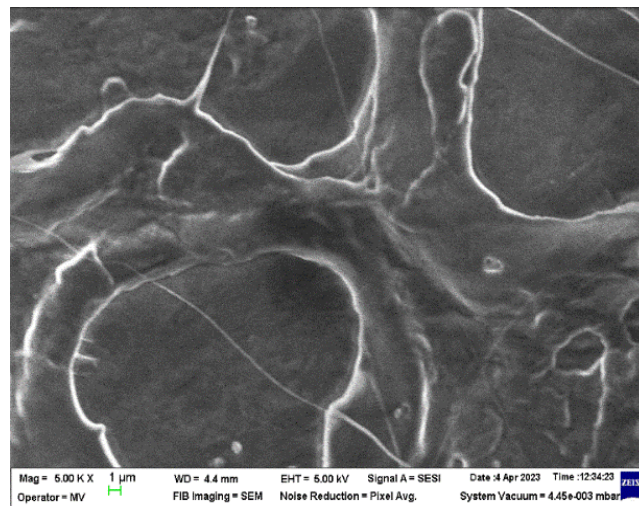


Figure 4. Microscopic image (5000 \times) for the PP polymeric material (M0) obtained through injection molding.

In the microscopic image of the M0 sample (Figure 4) the true state of the PP polymer can be observed as a blank surface only with an amorphous rheological morphology due to the injection molding process. The microscopic images of the M1-M4 samples (Figure 5) show different distribution behavior of SrFe₁₂O₁₉ filler in the PP polymer matrix.

After analyzing the micrographs performed on the composite materials (Figure 5), it can be observed that the M1 and M2 materials have higher homogeneity compared to the M3 and M4 materials with ferrite concentrate filler. This behavior is caused by the presence of the PA12 polymer existent in the filler concentrate, which has a higher melt flow index (Table 3) than the one of the PP polymer matrix (Table 1). The decrease in homogeneity is visible in the micrographs in the form of cluster-like agglomerates of ferrite particles in the PP polymer matrix.

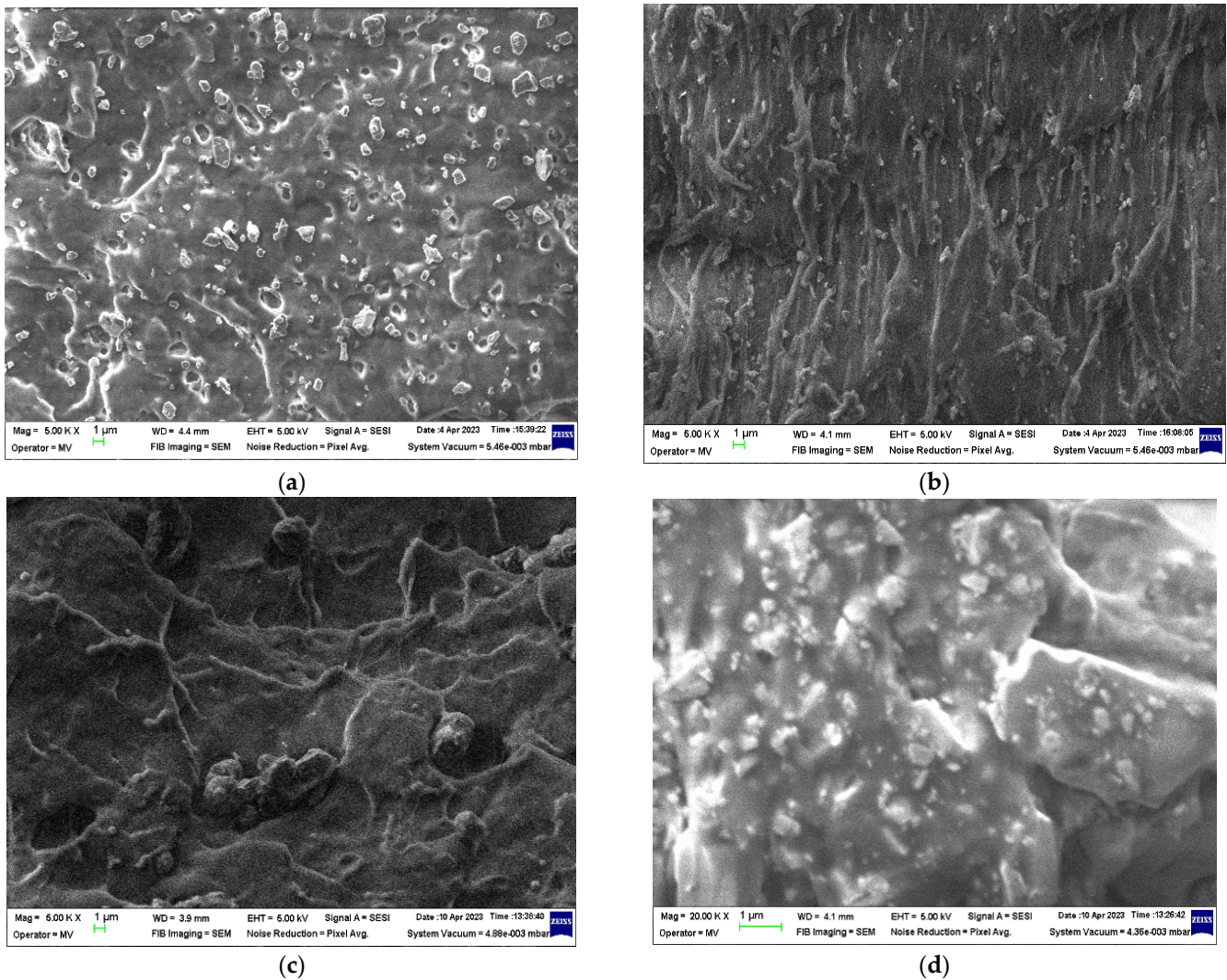


Figure 5. Microscopic images (5000 \times for (a–c) and 20,000 \times for (d)) for the PP/SrFe₁₂O₁₉ polymer composite materials: (a) M1, (b) M2, (c) M3, and (d) M4 obtained through injection molding.

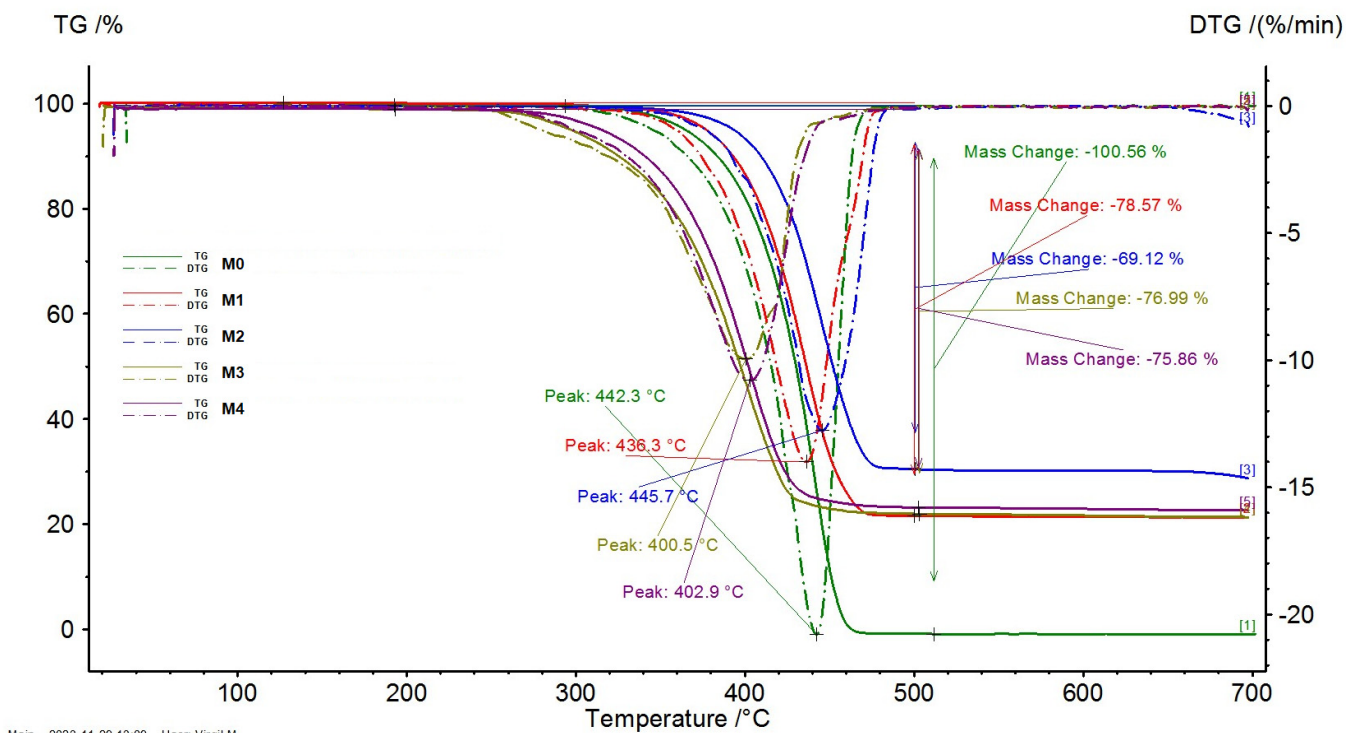
3.4. Thermal Analysis

Figure 6 presents the TG and DTG curves of the M0–M4 materials obtained through injection molding.

The decomposition process of the PP polymer (M0) is at its maximum at 442.3 °C, while for the PP/SrFe₁₂O₁₉ polymer composite materials (M1–M4), this is dependent on the quantity and type of the utilized filler.

The decomposition process of the composite materials with ferrite powder filler (M1 and M2) presents a maximum at 436.3 °C and 445.7 °C, respectively. On the other hand, the decomposition process of the materials with the F1-type ferrite concentrate filler (M3 and M4) presents a maximum at 400.5 °C and 402.9 °C, respectively. The decrease in the maximum of the decomposition process is determined by the presence of nitrogen atoms existent in the composition of the polyamide (PA) polymer.

In Figure 6, it can be noticed that after 450 °C, all the polymers are decomposed in the volatile matter and the resulting solid residue consists of ferrite filler. The mass loss is around 100% for the PP polymer (M0), whereas for the polymer composite materials (M1–M4), it ranges between 69% and 79%. The obtained mass loss values are in line with the designed content of the ferrite filler.



Main 2023-11-29 13:09 User: Virgil.M

Figure 6. TG and DTG curves of the M0-M4 materials obtained through injection molding.

3.5. Dielectric Properties

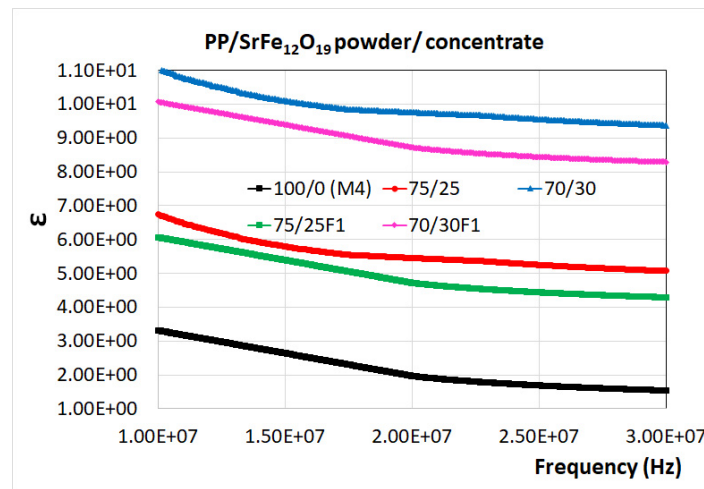
Figure 7 shows the variations of the tangent of the dielectric loss angle ($\text{tg } \delta$) and electrical conductivity (σ) over the frequency range of 8–30 MHz for the studied composite materials (M1-M4) compared to the PP polymeric material (M0). The frequency interval was particularly chosen to respond to the need for electromagnetic shielding from the electromagnetic radiation emitted mainly by exterior sources—electrical lines and supply sources—in terms of the development of the new electrical vehicles [67], for which particular testing equipment is in the process of development [68].

When analyzing the experimental data obtained for ϵ , $\text{tg } \delta$, and σ for the composite materials with fillers (M1-M4) comparatively with the PP polymer (Figure 7), it can be observed that the addition of $\text{SrFe}_{12}\text{O}_{19}$ powder/concentrate fillers leads to an increase mainly with regard to dielectric permittivity, but also with regard to both dielectric losses and electrical conductivities. Regarding the values of $\text{tg } \delta$ and σ for the recycled polypropylene (around 10^{-4} and 10^{-9} , respectively), they are very low compared to the composite values, seen at the base of the graphics.

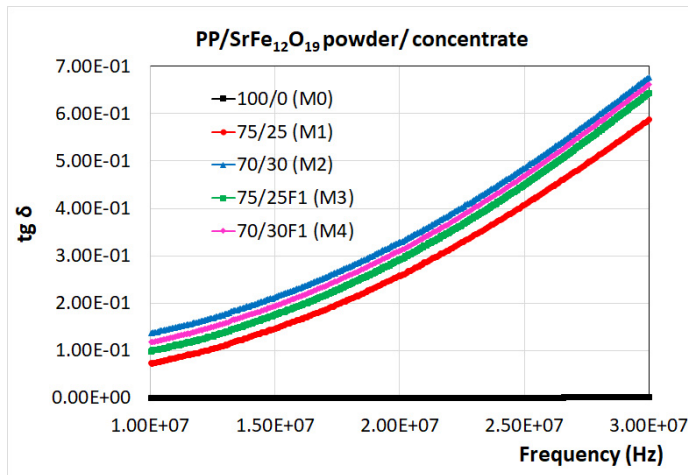
Additionally, the ϵ , $\text{tg } \delta$, and σ values of all the materials increased with the increase in frequency, in the series: M0, M1, M3, M4, and M2. The variation in the dielectric properties of polymer composites with frequency is typically ascribed to the dipole and interfacial polarization between the conductive filler and the polymer matrix, as well as to the relaxation mechanisms [34].

The M2 and M4 materials with the highest percentage (30 wt.%) in $\text{SrFe}_{12}\text{O}_{19}$ powder/concentrate show the greatest increases in electrical conductivity. Therefore, the obtained composite materials can be used as shielding materials since they are conductive and, thus, can contribute to the reflection mechanism of EMI shielding [34]. It is also noticed that the composite materials containing $\text{SrFe}_{12}\text{O}_{19}$ powder provide a better conductivity compared to that offered by the F1-type $\text{SrFe}_{12}\text{O}_{19}$ concentrate due to the achievement of homogeneous microstructure with uniform distribution of the filler particles into the polypropylene (PP) polymer matrix. The presence of the polyamide (PA) in the walls of the F1-type ferrite concentrate, a technology taken into account for the purpose of increasing the affinity of powders towards the PP matrix and diminishing flocculation effects, in fact

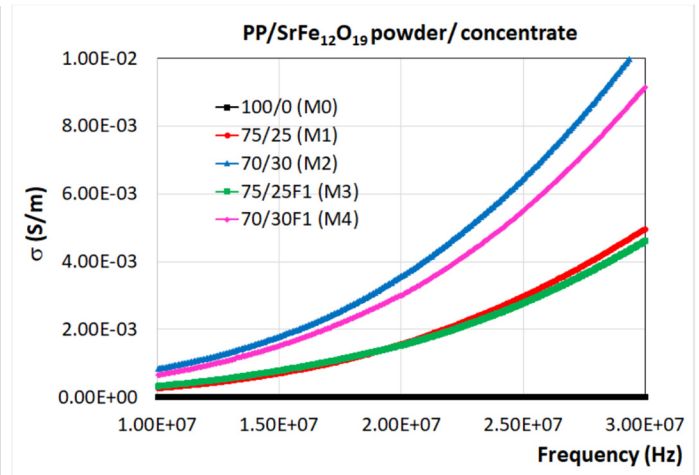
determined the decrease in the electrical conductivity of the composite materials, since the PA walls are insulators with very low conductivity.



(a)



(b)



(c)

Figure 7. Variation in (a) relative dielectric permittivity (ϵ); (b) tangent of dielectric loss angle ($\text{tg } \delta$); and (c) electrical conductivity (σ) for the studied composite materials (M1-M4) compared to the PP polymeric material (M0).

3.6. Temperature Resistance

Temperature resistance testing was carried out by analyzing the variation in $\text{tg } \delta$ and electrical resistivity of all the samples subjected to accelerated aging (eight heating/cooling cycles) at 70 °C for 72 h/cycle and estimating, via calculations, the critical electrical resistivity and time at which the material can be considered degraded.

The variation in the electrical resistivity of the developed samples versus the exposure time at a temperature of 70 °C is presented in Figure 8, along with the first-degree equations ($y = ax + b$) that describe the trend of the variation curve.

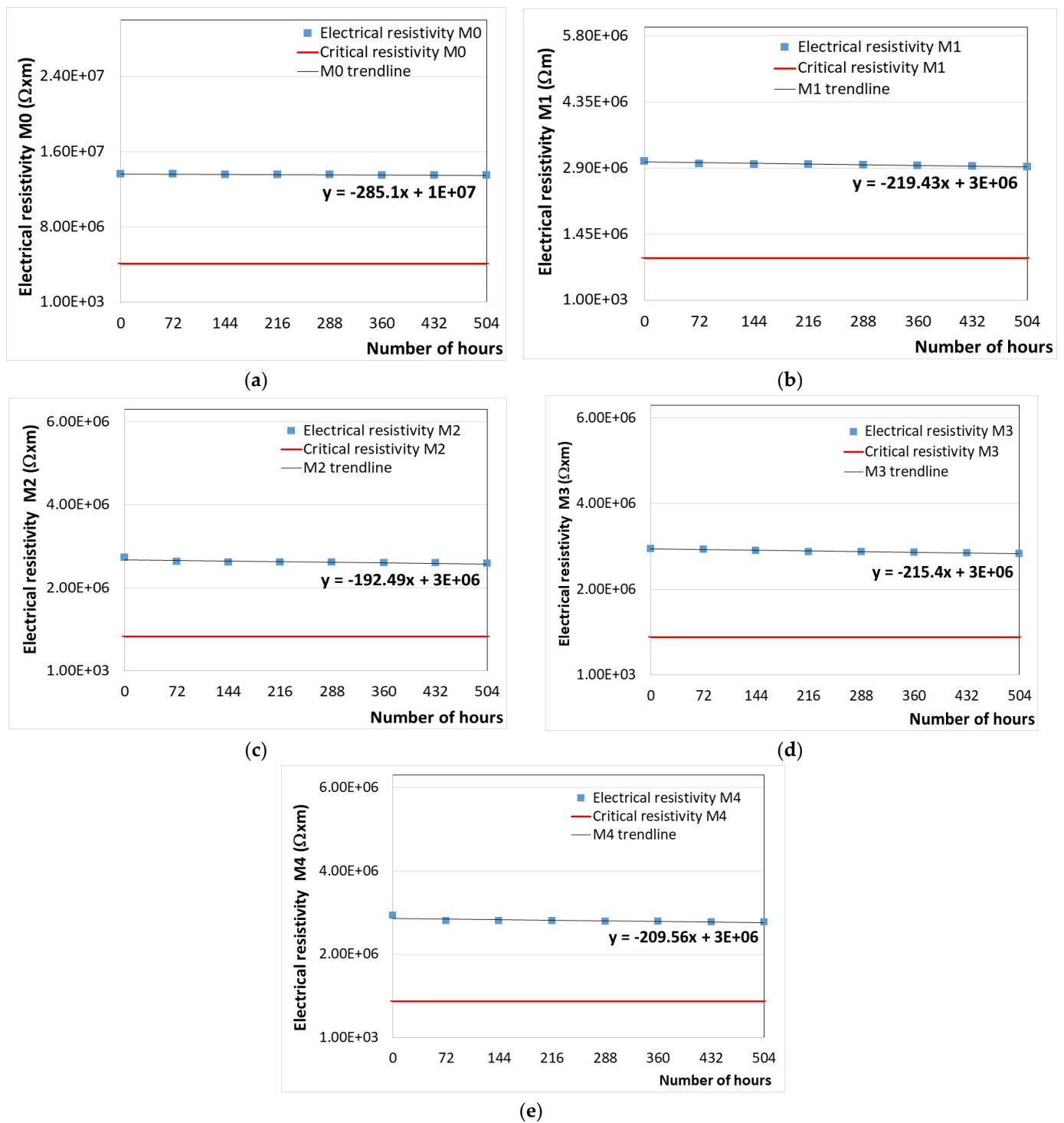


Figure 8. (a–e) Variation in the electrical resistivity of M0–M4 versus the exposure time at a temperature of 70 °C.

Using first-degree equations for calculating the solutions of the equations given by each graph shown in Figure 8, we obtained the data from Table 7. Thus, the number of hours of thermal aging can be identified in a facile way. This information is very useful in industrial applications to replace, at an appropriate time, the PP polymer-based materials subjected to thermal degradation.

Table 7. Results for determining the critical electrical resistivity and time at which the developed materials can be considered degraded after thermal aging at 70 °C.

Material Code	Equation	Critical Electrical Resistivity ($\Omega \cdot m$)	Critical Time (h)	Critical Time (days)
M0	$y = -285.1x + 1 \times 10^7$	4,084,298	20,750	865
M1	$y = -219.43x + 3 \times 10^6$	917,492	9491	395
M2	$y = -192.49x + 3 \times 10^6$	820,393	11,323	472
M3	$y = -215.4x + 3 \times 10^6$	884,210	9823	409
M4	$y = -209.56x + 3 \times 10^6$	879,685	10,118	422

According to the results shown in Table 7, we can estimate the time for the replacement of the PP polymer and PP/SrFe₁₂O₁₉ composite materials before reaching their irreparable damage and the end of protection from electromagnetic radiation. Thus, it is found that the number of days after which the materials have to be replaced is 865 days for M0, 395 days for M1, 472 days for M2, 409 days for M3, and 422 days for M4.

It must be mentioned that the values achieved as above are related to the thermal exposure of materials according to the electrical engineering standard [69], i.e., related to the insulation class; in our case, they were assimilated to the lowest insulation class A for automotive electronics—carcasses, etc. (105 °C limit of use, 70 °C exposure to determine lifetime, and 40 °C maximum ambient temperature), herewith M2 and M4 exceeding 10,000 h for 70 °C exposure. Regarding the real lifetime for automotive applications, the maximum ambient temperature must be taken into account, i.e., 40 °C, and applying the Arrhenius equation for accelerated thermal tests, e.g., as described in [70], the real service values are obtained by extrapolating the data from Table 7, exceeding 10 years of normal usage for M2 and M4.

Comparing the composite materials with SrFe₁₂O₁₉ fillers from the point of view of the maintenance time of the electromagnetic shield characteristics, the following classification can be made: M2 > M4 > M3 > M1. However, the M0 material made of PP polymer exhibited the highest temperature resistance over those of the PP/SrFe₁₂O₁₉ composite materials. The reason for a lower value of lifetime for M4 compared to M2 may be related to the obtaining process of the composites in two stages, finalized by melt injection, when mutual interactions between the SrFe₁₂O₁₉ particles and polymer matrix can occur on the filler–polymer interface in the melt PP polymer/ferrite mixture, which may cause slight repulsive forces due to the different affinity of inorganic particles to polymer matrix, as described, e.g., in [31].

3.7. Magnetic Properties

The determination of the complex magnetic permeability of the developed materials was carried out in the range of 8–30 MHz. The real magnetic permeability (μ') and tangent of the magnetic loss angle ($\text{tg } \delta = \mu''/\mu'$) values are presented in Figure 9.

All the PP/SrFe₁₂O₁₉ polymer composite materials (M1–M4) exhibited superior values of the real magnetic permeability (μ') than that of the PP polymer material (M0) over the studied frequency range. The μ' values were highly influenced by the content and distribution of the magnetic SrFe₁₂O₁₉ filler in the PP polymer matrix. The M2 material with the highest content of ferrite powder filler (30 wt.%) and homogeneous structure (Figure 5) exhibited the highest real magnetic permeability. In the case of the M4 material prepared with 30 wt.% ferrite concentrate filler, the real magnetic permeability is less than that for M2, due to the presence of the polyamide (PA) polymer in the walls of the F1-type filler concentrate which has a lower magnetic permeability.

The tangent of magnetic loss angle was higher for the M4 material for frequencies exceeding 20 MHz, followed by the M2 material, while the other materials exhibited a lower comparative behavior over the whole frequency range.

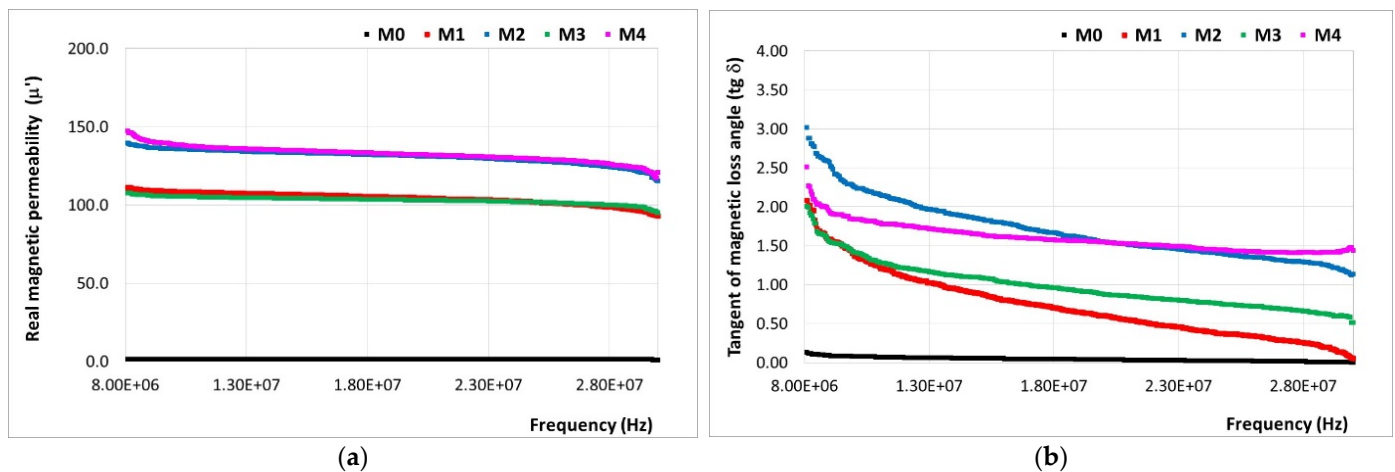


Figure 9. Variation in (a) real magnetic permeability (μ') and (b) tangent of magnetic loss angle ($\text{tg } \delta$) for the studied composite materials (M1-M4) compared to the PP polymeric material (M0).

On the other hand, it can be observed that the addition of $\text{SrFe}_{12}\text{O}_{19}$ powder into the PP polymer matrix does not lead to better magnetic loss along all frequency domains, as it was noticed for dielectric loss when compared to the addition of the $\text{SrFe}_{12}\text{O}_{19}$ concentrate. This difference is explained by the fact that, when taking into account the dielectric loss, the obtaining of composites using $\text{SrFe}_{12}\text{O}_{19}$ concentrate as a filler (M3 and M4), homogenization with the polypropylene (PP) polymer matrix is hampered by the polyamide (PA) existent in the F1-type ferrite concentrate, which is not fully miscible with polypropylene and may involve repulsive forces that may lead to the appearance of defects, resulting in a continuous decrease in dielectric parameters in all frequency domains, aspect negligible when speaking about magnetic parameters.

4. Conclusions

In this work, recycled polypropylene/strontium ferrite (PP/ $\text{SrFe}_{12}\text{O}_{19}$) polymer composite materials were analyzed, with potential applications in electromagnetic shielding (mainly automotive electronics—carcasses) from the electromagnetic radiation emitted mainly by exterior sources—electrical lines and supply sources—in terms of the development of the new electrical vehicles.

The recycled polypropylene was particularly analyzed, due to the unification of polymer matrices used/to be further used in automotive applications; hereby, polypropylene was appointed, and in terms of Directive 2000/53/EU on end-of-life vehicles [71], one of the requirements is that a minimum of 25% of the plastic used to build a new vehicle must be recycled. On the other hand, an important reason for choosing strontium ferrites is that they are low-cost, widely used for ferrite permanent magnets, and may also become an important source of recycled matter in the near future.

The composites were obtained in two stages, i.e., pellets by extrusion and samples for testing via a melt injection process and characterized comparatively with the PP polymer used as a matrix. The composite materials were prepared with $\text{SrFe}_{12}\text{O}_{19}$ filler in powder/concentrate form with mass concentrations expressed by the PP/ $\text{SrFe}_{12}\text{O}_{19}$ ratio of 100/0, 75/25, and 70/30. The obtained materials were coded as M0 for the PP polymer, M1 and M2 for the materials with ferrite powder filler, and M3 and M4 for the materials with ferrite concentrate filler, with polyamide cover, a technology taken into account for the purpose of increasing the affinity of powders towards polypropylene matrix and diminishing flocculation effects.

The characterization of the developed materials involved the determination of relevant physical, mechanical, dielectric, thermal, magnetic, and electromagnetic properties, as well as the study of the microstructure.

The macrographic aspect and density values of $(1.068\text{--}1.157) \pm 0.002 \text{ g/cm}^3$ show the obtaining of uniform, homogeneous, and lightweight PP/ferrite polymer composite materials (M1-M4) via the utilized preparation methods. The composite materials with $\text{SrFe}_{12}\text{O}_{19}$ powder filler exhibited higher density than the materials with $\text{SrFe}_{12}\text{O}_{19}$ filler concentrate at the same content of filler. The filler addition increased by about 20–29% the density of the M1-M4 materials compared to the density of the PP polymer (M0).

The nanoindentation tests performed on the injection-molded materials disclosed an improvement in the mechanical properties due to the $\text{SrFe}_{12}\text{O}_{19}$ filler addition to the PP matrix. The indentation hardness (H_{IT}) and Vickers hardness, as well as the indentation elastic modulus (E_{IT}) and contact stiffness (S), increased with the filler content increase.

The contribution of the $\text{SrFe}_{12}\text{O}_{19}$ powder filler toward the enhancement of the mechanical properties was higher than in the case of using the $\text{SrFe}_{12}\text{O}_{19}$ concentrate filler, which is a compound containing HM 1213—polyamide 12 (PA12) and 85% $\text{SrFe}_{12}\text{O}_{19}$ powder. The PP polymer (M0) exhibited the lowest hardness, elastic modulus, and contact stiffness. On the contrary, this material exhibited the highest W_{elast} and η_{IT} values indicating a higher elastic deformation ability due to preserving the polymer chain structure in case no filler is added to the polymer matrix. The creep behavior of the M0, M3, and M4 materials with PP and 25–30 wt.% PP/ $\text{SrFe}_{12}\text{O}_{19}$ concentrate is similar, but the creep resistance was better for the composites with a lower content of $\text{SrFe}_{12}\text{O}_{19}$ filler.

All the M0-M1 materials exhibited a similar viscoelastic behavior showing higher W_{plast} values than the W_{elast} ones. It was also noticed that the M2 material exhibited higher plastic behavior than the other materials. According to the results of the mechanical tests performed, the M2 composite material was chosen as the optimal variant.

The SEM analysis performed on the injection-molded materials revealed the true state of the PP polymeric material (M0) as a blank surface only with an amorphous rheological morphology, whereas the M1-M4 materials show different $\text{SrFe}_{12}\text{O}_{19}$ filler distribution behavior in the polypropylene (PP) polymer matrix. The M1 and M2 materials have higher homogeneity compared to the M3 and M4 materials with ferrite concentrate filler containing PA12 polymer with a higher melt flow index than the one of the PP polymer matrix. The decrease in the homogeneity of composite materials is visible in the micrographs as cluster-like agglomerates of ferrite particles in the PP polymer matrix.

The decomposition process of the PP polymer (M0) is at its maximum at 442.3 °C, while for the PP/ $\text{SrFe}_{12}\text{O}_{19}$ polymer composite materials (M1-M4), this is dependent on the quantity and type of the utilized filler. The decomposition process of the M1 and M2 materials with ferrite powder filler presents a maximum at 436.3 °C and 445.7 °C, respectively. The decomposition process of the M3 and M4 materials with ferrite concentrate filler presents a maximum at 400.5 °C and 402.9 °C, respectively, caused by the presence of nitrogen atoms existent in the composition of the polyamide polymer. After 450 °C, all the polymers are decomposed in the volatile matter and the resulting solid residue consists of ferrite filler. The mass loss is around 100% for the PP polymer (M0) and in the range of 69–79% for the M1-M4 composite, which is in line with the designed content of the ferrite filler.

The dielectric tests performed on these composite materials over the frequency range of 8–30 MHz qualify the composite material coded with M2 as the material with the highest electrical conductivity (σ) among the analyzed materials. The addition of 30 wt.% $\text{SrFe}_{12}\text{O}_{19}$ powder into the PP matrix increased the conductivity of the M2 material compared to that of the M4 material made of PP and the same content of the F1-type ferrite concentrate. The decrease in electrical conductivity resulted from the presence of the polyamide (PA) in the walls of the ferrite concentrate. The PA walls are insulators with very low electrical conductivity which also induces in the M4 material a lower conductivity compared to that of the M2 material in which only polypropylene (PP) polymer appears.

The results obtained for the temperature resistance testing by investigating the thermal aging behavior of materials (eight heating/cooling cycles) at 70 °C for 72 h/cycle indicated the number of days after which the materials have to be replaced. The most

temperature-resistant composite material was found to be the M2 material. The values achieved as above are related to the thermal exposure of materials according to the electrical engineering standard, i.e., related to the insulation class, in our case, they were assimilated to the lowest insulation class A for automotive electronics—carcasses, etc. (105 °C limit of use, 70 °C exposure to determine lifetime, and 40 °C maximum ambient temperature), herewith M2 and M4 exceeding 10,000 h for 70 °C exposure. Regarding the real lifetime for automotive applications, the maximum ambient temperature must be taken into account, i.e., 40 °C, and applying the Arrhenius equation for accelerated thermal tests, the real service values obtained through extrapolation exceeded 10 years of normal usage for M2 and M4.

Regarding the obtained magnetic permeability and the magnetic loss, it can be concluded that both the M2 and M4 materials present high performance along the entire frequency field; however, M2 may be preferred, due to the fact that when obtaining composites using SrFe₁₂O₁₉ concentrate as a filler (M3 and M4), homogenization with the polypropylene (PP) polymer matrix is hampered by the polyamide (PA) existent in the F1-type ferrite concentrate, which is not fully miscible with polypropylene and may involve repulsive forces that may lead to the appearance of defects, resulting in a continuous decrease in dielectric parameters in all frequency domain, aspect negligible when speaking about magnetic parameters.

The promising results recommend the M2 polymer composite material for potential use in shielding applications against electromagnetic pollution, but further studies are necessary for the upscaling of the material in real-size applications, along with a precise analysis of the electromagnetic shielding effect.

Author Contributions: Conceptualization, A.R.C. and R.C.C.; methodology, R.C.C., A.R.C. and I.I.; software, O.D.S.; validation, R.C.C., O.D.S. and A.R.C.; formal analysis, A.R.C. and I.I.; investigation, A.R.C., M.V.L., I.I., J.P., M.M., S.A. and V.M.; resources, A.R.C., I.I. and R.C.C.; data curation, A.R.C., M.V.L., I.I., M.M., S.A. and V.M.; writing—original draft preparation, A.R.C., I.I. and R.C.C.; writing—review and editing, A.R.C., M.V.L., I.I. and R.C.C.; visualization, R.C.C. and A.R.C.; supervision, R.C.C.; funding acquisition, R.C.C. All authors have read and agreed to the published version of the manuscript.

Funding: This work was supported by a publication grant from the Technical University of Iasi, and it was based on the joint experimental research of participating organizations, partially financed on the part of the National Institute for Research and Development in Electrical Engineering ICPE-CA Bucharest by the Romanian Ministry of Research, Innovation and Digitalization, project number 25PFE/30.12.2021—Increasing R-D-I capacity for electrical engineering-specific materials and equipment with reference to electromobility and “green” technologies within PNCDI III, Programme 1.

Institutional Review Board Statement: Not applicable.

Informed Consent Statement: Not applicable.

Data Availability Statement: Data are contained within the article.

Conflicts of Interest: The authors declare no conflicts of interest.

References

1. Kim, J.K.; Kang, S.-S.; Kim, H.G.; Kwac, L.K. Mechanical Properties and Electromagnetic Interference Shielding of Carbon Composites with Polycarbonate and Acrylonitrile Butadiene Styrene Resins. *Polymers* **2023**, *15*, 863. [[CrossRef](#)]
2. Tian, K.; Hu, D.; Wei, Q.; Fu, Q.; Deng, H. Recent Progress on Multifunctional Electromagnetic Interference Shielding Polymer Composites. *J. Mater. Sci. Technol.* **2023**, *134*, 106–131. [[CrossRef](#)]
3. Shukla, V. Review of Electromagnetic Interference Shielding Materials Fabricated by Iron Ingredients. *Nanoscale Adv.* **2019**, *1*, 1640–1671. [[CrossRef](#)] [[PubMed](#)]
4. Sayed, W.E.; Lezynski, P.; Smolenski, R.; Moonen, N.; Crovetto, P.; Thomas, D.W.P. The Effect of EMI Generated from Spread-Spectrum-Modulated SiC-Based Buck Converter on the G3-PLC Channel. *Electronics* **2021**, *10*, 1416. [[CrossRef](#)]
5. Apakuppakul, S.; Methachittiphan, N.; Apiyasawat, S. Effect of ElectroMagnetic Interference from SmartPHONE on Cardiac ImplaNtable Electronic Device (EMI-PHONE Study). *J. Arrhythm.* **2022**, *38*, 778–782. [[CrossRef](#)] [[PubMed](#)]

6. Wang, J.; Wang, H.; Sun, Z. Research on the Effectiveness of Deep Convolutional Neural Network for Electromagnetic Interference Identification Based on I/Q Data. *Atmosphere* **2022**, *13*, 1785. [[CrossRef](#)]
7. Okechukwu, C. Effects of Radiofrequency Electromagnetic Field Exposure on Neurophysiology. *Adv. Hum. Biol.* **2020**, *10*, 6. [[CrossRef](#)]
8. Razek, A. Biological and Medical Disturbances Due to Exposure to Fields Emitted by Electromagnetic Energy Devices—A Review. *Energies* **2022**, *15*, 4455. [[CrossRef](#)]
9. Bolte, J.F.B.; Baliatsas, C.; Eikelboom, T.; Van Kamp, I. Everyday Exposure to Power Frequency Magnetic Fields and Associations with Non-Specific Physical Symptoms. *Environ. Pollut.* **2015**, *196*, 224–229. [[CrossRef](#)]
10. Hwang, J.-H.; Kang, T.-W.; Kwon, J.-H.; Park, S.-O. Effect of Electromagnetic Interference on Human Body Communication. *IEEE Trans. Electromagn. Compat.* **2017**, *59*, 48–57. [[CrossRef](#)]
11. Baliatsas, C.; Van Kamp, I.; Bolte, J.; Schipper, M.; Yzermans, J.; Lebret, E. Non-Specific Physical Symptoms and Electromagnetic Field Exposure in the General Population: Can We Get More Specific? A Systematic Review. *Environ. Int.* **2012**, *41*, 15–28. [[CrossRef](#)] [[PubMed](#)]
12. Szemerszky, R.; Zelena, D.; Barna, I.; Bárdos, G. Stress-Related Endocrinological and Psychopathological Effects of Short- and Long-Term 50Hz Electromagnetic Field Exposure in Rats. *Brain Res. Bull.* **2010**, *81*, 92–99. [[CrossRef](#)]
13. Agarwal, J.; Sahoo, S.; Mohanty, S.; Nayak, S.K. Progress of Novel Techniques for Lightweight Automobile Applications through Innovative Eco-Friendly Composite Materials: A Review. *J. Thermoplast. Compos. Mater.* **2020**, *33*, 978–1013. [[CrossRef](#)]
14. Radu, E.; Lipcinski, D.; Tanase, N.; Lingvay, I. The Influence of the 50 Hz Electric Field on the Development and Maturation of *Aspergillus Niger*. *Electroteh. Electron. Autom.* **2015**, *63*, 68–74.
15. Stancu, C.; Lingvay, M.; Szatmari, I.; Lingvay, I. Influence of 50 Hz Electromagnetic Field on the Yeast (*Saccharomyces Cerevisiae*) Metabolism. In Proceedings of the 2013 8th International Symposium on Advanced Topics in Electrical Engineering (ATEE), Bucharest, Romania, 23–25 May 2013; IEEE: Bucharest, Romania, 2013; pp. 1–4. [[CrossRef](#)]
16. Beyza, H.U.; Nejat, S.H.; Fatma, K.Y. Heat-resistant moulds: Assessment, prevention and their consequences for food safety and public health. *Czech J. Food Sci.* **2022**, *40*, 273–280. [[CrossRef](#)]
17. Zhang, M.; Han, C.; Cao, W.-Q.; Cao, M.-S.; Yang, H.-J.; Yuan, J. A Nano-Micro Engineering Nanofiber for Electromagnetic Absorber, Green Shielding and Sensor. *Nano-Micro Lett.* **2021**, *13*, 27. [[CrossRef](#)] [[PubMed](#)]
18. Quan, B.; Shi, W.; Ong, S.J.H.; Lu, X.; Wang, P.L.; Ji, G.; Guo, Y.; Zheng, L.; Xu, Z.J. Defect Engineering in Two Common Types of Dielectric Materials for Electromagnetic Absorption Applications. *Adv. Funct. Mater.* **2019**, *29*, 1901236. [[CrossRef](#)]
19. Lingvay, M.; Caramitu, A.-R.; Bors, A.-M.; Lingvay, I. Dielectric Spectroscopic Evaluation in the Extremely Low Frequency Range of an *Aspergillus Niger* Culture. *Stud. UBB Chem.* **2019**, *64*, 279–288. [[CrossRef](#)]
20. Sandu, D.; Lingvay, I.; Szabolcs, L.; Micu, D.D.; Popescu, C.; Jurgen, B.; Bartha, C.; Csaba, P. The Effect of Electromagnetic Fields on Baker's Yeast Population Dynamics, Biocatalytic Activity and Selectivity. *Stud. UBB Chem.* **2009**, *LIV*, 195–201.
21. Bors, A.M.; Butoi, N.; Caramitu, A.R.; Marinescu, V.; Lingvay, I. The Thermooxidation and Resistance to Moulds Action of Some Polyethylene Sorts Used at Anticorrosive Insulation of the Underground Pipelines. *Mat. Plast.* **2017**, *54*, 447–452. [[CrossRef](#)]
22. Bartha, C.; Caramitu, A.; Jipa, M.; Ignat, D.M.; Tókos, A. Dielectric Behavior of Sludge from Waste Water Treatment. *Stud. UBB Chem.* **2020**, *65*, 85–93. [[CrossRef](#)]
23. Tokos, A.; Bartha, C.; Jipa, M.; Micu, D.-D.; Caramitu, A.-R.; Lingvay, I. Interactions of Extremely Low-Frequency Electric Field with the Active Sludge Live Materia from Wastewater Treatments. In Proceedings of the 2021 12th International Symposium on Advanced Topics in Electrical Engineering (ATEE), Bucharest, Romania, 25–27 March 2021; IEEE: Bucharest, Romania, 2021; pp. 1–4. [[CrossRef](#)]
24. Kalia, S.; Kango, S.; Kumar, A.; Haldorai, Y.; Kumari, B.; Kumar, R. Magnetic Polymer Nanocomposites for Environmental and Biomedical Applications. *Colloid Polym. Sci.* **2014**, *292*, 2025–2052. [[CrossRef](#)]
25. Lingvay, I.; Voina, A.; Lingvay, C.; Mateescu, C. The Impact of the Electromagnetic Pollution of the Environment on the Complex Build-up Media. *Rev. Roum. Sci. Techn.—Électrotechn. Énerg.* **2008**, *53*, 95–111.
26. Rus, T.; Bors, A.M.; Caramitu, A.R.; Lingvay, I.; Vaicanu, D.I. Comparative Studies on the Thermal Ageing of Some Painting Materials. *Mat. Plast.* **2018**, *55*, 168–175. [[CrossRef](#)]
27. Wang, X.-X.; Zhang, M.; Shu, J.-C.; Wen, B.; Cao, W.-Q.; Cao, M.-S. Thermally-Tailoring Dielectric “Genes” in Graphene-Based Heterostructure to Manipulate Electromagnetic Response. *Carbon* **2021**, *184*, 136–145. [[CrossRef](#)]
28. Bors, A.-M.; Lingvay, D.; Caramitu, A.-R.; Iordache, I.; Lingvay, I. Comparative Studies on the Electrical and Mechanical Behavior of Some Soldering and/or Impregnation Lacquers. *Mat. Plast.* **2019**, *56*, 129–132. [[CrossRef](#)]
29. Sanida, A.; Stavropoulos, S.G.; Speliotis, T.; Psarras, G.C. Investigating the Effect of Zn Ferrite Nanoparticles on the Thermomechanical, Dielectric and Magnetic Properties of Polymer Nanocomposites. *Materials* **2019**, *12*, 3015. [[CrossRef](#)] [[PubMed](#)]
30. Radoń, A.; Hawełek, Ł.; Łukowiec, D.; Kubacki, J.; Włodarczyk, P. Dielectric and Electromagnetic Interference Shielding Properties of High Entropy (Zn,Fe,Ni,Mg,Cd)Fe₂O₄ Ferrite. *Sci. Rep.* **2019**, *9*, 20078. [[CrossRef](#)]
31. Kruželák, J.; Kvasničáková, A.; Hložeková, K.; Dosoudil, R.; Gořalík, M.; Hudec, I. Electromagnetic Interference Shielding and Physical-Mechanical Characteristics of Rubber Composites Filled with Manganese-Zinc Ferrite and Carbon Black. *Polymers* **2021**, *13*, 616. [[CrossRef](#)]
32. Li, Z.W.; Yang, Z.H. The Studies of High-Frequency Magnetic Properties and Absorption Characteristics for Amorphous-Filler Composites. *J. Magn. Magn. Mater.* **2015**, *391*, 172–178. [[CrossRef](#)]

33. Yakovenko, O.S.; Matzui, L.Y.; Vovchenko, L.L.; Lazarenko, O.A.; Perets, Y.S.; Lozitsky, O.V. Complex Permittivity of Polymer-Based Composites with Carbon Nanotubes in Microwave Band. *Appl. Nanosci.* **2020**, *10*, 2691–2697. [CrossRef]
34. Kruželák, J.; Kvasničáková, A.; Hložeková, K.; Hudec, I. Progress in Polymers and Polymer Composites Used as Efficient Materials for EMI Shielding. *Nanoscale Adv.* **2021**, *3*, 123–172. [CrossRef]
35. Kumar, P.; Narayan Maiti, U.; Sikdar, A.; Kumar Das, T.; Kumar, A.; Sudarsan, V. Recent Advances in Polymer and Polymer Composites for Electromagnetic Interference Shielding: Review and Future Prospects. *Polym. Rev.* **2019**, *59*, 687–738. [CrossRef]
36. Li, B.-W.; Shen, Y.; Yue, Z.-X.; Nan, C.-W. Enhanced Microwave Absorption in Nickel/Hexagonal-Ferrite/Polymer Composites. *Appl. Phys. Lett.* **2006**, *89*, 132504. [CrossRef]
37. Turchenko, V.A.; Trukhanov, A.; Trukhanov, S.; Damay, F.; Porcher, F.; Balasoïu, M.; Lupu, N.; Chiriac, H.; Bozzo, B.; Fina, I.; et al. Magnetic and Ferroelectric Properties, Crystal and Magnetic Structures of SrFe_{11.9}In_{0.1}O₁₉. *Phys. Scr.* **2020**, *95*, 044006. [CrossRef]
38. Lee, S.H.; Jeung, W.Y. Anisotropic Injection Molding of Strontium Ferrite Powder Using a PP/PEG Binder System. *J. Magn. Magn. Mater.* **2001**, *226–230*, 1400–1402. [CrossRef]
39. Hemedá, O.M.; Henaish, A.M.A.; Salem, B.I.; El-Sbakhly, F.S.; Hamad, M.A. The Dielectric and Magnetic Properties of RTV-Silicon Rubber Ni–Cr Ferrite Composites. *Appl. Phys. A* **2020**, *126*, 121. [CrossRef]
40. Al-Nesraway, S.H.; Al-Maamori, M.H.; Al-Issawe, J.M. Preparation of a Rubber Nanocomposite (Silicone Rubber-Ferrite) for Protect Human from Bioeffects of Microwave Emitted from Mobile Devices. *J. Bionanosci.* **2018**, *12*, 645–651. [CrossRef]
41. Kruželák, J.; Matvejevová, M.; Dosoudil, R.; Hudec, I. Barium and Strontium Ferrite-Filled Composites Based on NBR and SBR. *J. Elastomers Plast.* **2019**, *51*, 421–439. [CrossRef]
42. Suprapedi; Muljadi; Ramlan. Effect of Silicon Rubber Composition on Mechanical and Magnetic Properties of Rubber Composite Sr-Ferrite Magnet. *AIP Conf. Proc.* **2020**, *2221*, 110005. [CrossRef]
43. Hema, S.; Sambhudevan, S. Ferrite-Based Polymer Nanocomposites as Shielding Materials: A Review. *Chem. Pap.* **2021**, *75*, 3697–3710. [CrossRef]
44. La Rosa, A.D.; Grammatikos, S.A.; Ursan, G.A.; Aradoaei, S.; Summerscales, J.; Ciobanu, R.C.; Schreiner, C.M. Recovery of Electronic Wastes as Fillers for Electromagnetic Shielding in Building Components: An LCA Study. *J. Clean. Prod.* **2021**, *280*, 124593. [CrossRef]
45. ISO 1133. Available online: <https://www.iso.org/standard/83905.html> (accessed on 10 November 2023).
46. ISO 1183. Available online: <https://www.iso.org/standard/74990.html> (accessed on 10 November 2023).
47. ISO 306. Available online: <https://magazin.asro.ro/ro/standard/280443> (accessed on 10 November 2023).
48. ASTM D638. Available online: <https://www.astm.org/d0638-14.html> (accessed on 10 November 2023).
49. ISO 179. Available online: <https://www.iso.org/obp/ui/#iso:std:iso:179:-1:ed-3:v1:en> (accessed on 10 November 2023).
50. ISO 178. Available online: <https://www.iso.org/standard/70513.html> (accessed on 10 November 2023).
51. ASTM D792; Standard Test Methods for Density and Specific Gravity (Relative Density) of Plastics by Displacement. ASTM: West Conshohocken, PA, USA, 2020.
52. ISO 14577-1. Available online: <https://www.iso.org/standard/56626.html> (accessed on 10 November 2023).
53. Oliver, W.C.; Pharr, G.M. An Improved Technique for Determining Hardness and Elastic Modulus Using Load and Displacement Sensing Indentation Experiments. *J. Mater. Res.* **1992**, *7*, 1564–1583. [CrossRef]
54. Lungu, M.V.; Lucaci, M.; Tsakiris, V.; Brătulescu, A.; Cîrstea, C.D.; Marin, M.; Pătroi, D.; Mitrea, S.; Marinescu, V.; Grigore, F.; et al. Development and Investigation of Tungsten Copper Sintered Parts for Using in Medium and High Voltage Switching Devices. *IOP Conf. Ser. Mater. Sci. Eng.* **2017**, *209*, 012012. [CrossRef]
55. Lungu, M.V.; Pătroi, D.; Marinescu, V.; Caramitu, A.; Marin, M.; Tălpeanu, D.; Lucaci, M.; Godeanu, P. Preparation and study of the optical, electrical and dielectric characteristics of some disc-shaped tin dioxide-based varistors. *Rom. J. Phys.* **2022**, *67*, 610.
56. Ding, Y.; Liu, W.; Cao, R.; Mei, C.; Wan, K.; Su, H.; Zhang, X.; Zou, Z.; Wang, J. Reductive Synthesis of Fe@Al₂O₃ Micro Powders with High Permeability and Low Magnetic Loss in the MHz Range. *J. Magn. Magn. Mater.* **2023**, *579*, 170865. [CrossRef]
57. Dhawan, S.K.; Ohlan, A.; Singh, K. Designing of Nano Composites of Conducting Polymers for EMI Shielding. In *Advances in Nanocomposites-Synthesis, Characterization and Industrial Applications*; Reddy, B., Ed.; InTech: London, UK, 2011. [CrossRef]
58. Wang, D.; Zhu, J.; Yao, Q.; Wilkie, C.A. A Comparison of Various Methods for the Preparation of Polystyrene and Poly(Methyl Methacrylate) Clay Nanocomposites. *Chem. Mater.* **2002**, *14*, 3837–3843. [CrossRef]
59. Weidenfeller, B.; Höfer, M.; Schilling, F.R. Cooling Behaviour of Particle Filled Polypropylene during Injection Moulding Process. *Compos. Part A Appl. Sci. Manuf.* **2005**, *36*, 345–351. [CrossRef]
60. Wypych, G. The Effect of Fillers on the Mechanical Properties of Filled Materials. In *Handbook of Fillers*; Elsevier: Amsterdam, The Netherlands, 2021; pp. 525–608. [CrossRef]
61. Banerjee, T.; Kar, S. Nanoindentation of Reinforced Polymer Composites. In *Encyclopedia of Materials: Plastics and Polymers*; Elsevier: Amsterdam, The Netherlands, 2022; pp. 688–699. [CrossRef]
62. Gibson, R.F. A Review of Recent Research on Nanoindentation of Polymer Composites and Their Constituents. *Compos. Sci. Technol.* **2014**, *105*, 51–65. [CrossRef]
63. Díez-Pascual, A.M.; Gómez-Fatou, M.A.; Ania, F.; Flores, A. Nanoindentation in Polymer Nanocomposites. *Prog. Mater. Sci.* **2015**, *67*, 1–94. [CrossRef]
64. Oliver, W.C.; Pharr, G.M. Measurement of Hardness and Elastic Modulus by Instrumented Indentation: Advances in Understanding and Refinements to Methodology. *J. Mater. Res.* **2004**, *19*, 3–20. [CrossRef]

65. Ovsik, M.; Stanek, M.; Dockal, A. Tribological and Micro-Mechanical Properties of Injected Polypropylene Modified by Electron Radiation. *Lubricants* **2023**, *11*, 296. [[CrossRef](#)]
66. Wang, J.; Yang, C.; Liu, Y.; Li, Y.; Xiong, Y. Using Nanoindentation to Characterize the Mechanical and Creep Properties of Shale: Load and Loading Strain Rate Effects. *ACS Omega* **2022**, *7*, 14317–14331. [[CrossRef](#)] [[PubMed](#)]
67. Available online: <https://www.sciencedirect.com/science/article/abs/pii/B9780128051931000173> (accessed on 10 November 2023).
68. Available online: <https://www.unitest.com/pdf/schwarzbeck/receiver/m1528en.pdf> (accessed on 10 November 2023).
69. *IEC 60034-1*; Insulation Class and Temperature Rise. IEC: Geneva, Switzerland, 2010.
70. Available online: <https://ieeexplore.ieee.org/document/9214671> (accessed on 10 November 2023).
71. Available online: https://environment.ec.europa.eu/topics/waste-and-recycling/end-life-vehicles_en (accessed on 10 November 2023).

Disclaimer/Publisher’s Note: The statements, opinions and data contained in all publications are solely those of the individual author(s) and contributor(s) and not of MDPI and/or the editor(s). MDPI and/or the editor(s) disclaim responsibility for any injury to people or property resulting from any ideas, methods, instructions or products referred to in the content.